Synthesis, X-ray Structure, Cytotoxic, and Anti-Microbial Activities of Zn(II) Complexes with a Hydrazono *s*-Triazine Bearing Pyridyl Arm

MennaAllah Hassan [1], Ayman El-Faham [1], Assem Barakat [2], Matti Haukka [3], Rajendhraprasad Tatikonda [3], Morsy A. M. Abu-Youssef [1], Saied M. Soliman [1,*] and Amal Yousri [1,*]

[1] Department of Chemistry, Faculty of Science, Alexandria University, P.O. Box 426, Ibrahimia, Alexandria 21321, Egypt; mennaallahhassanelsayed@gmail.com (M.H.); ayman.elfaham@alexu.edu.eg or aymanel_faham@hotmail.com (A.E.-F.); morsy5@alexu.edu.eg (M.A.M.A.-Y.)

[2] Department of Chemistry, College of Science, King Saud University, P.O. Box 2455, Riyadh 11451, Saudi Arabia; ambarakat@ksu.edu.sa

[3] Department of Chemistry, University of Jyväskylä, P.O. Box 35, FI-40014 Jyväskylä, Finland; matti.o.haukka@jyu.fi (M.H.); rp.tatikonda@jyu.fi (R.T.)

* Correspondence: saied1soliman@yahoo.com or saeed.soliman@alexu.edu.eg (S.M.S.); amal.yousri@alexu.edu.eg or amalyousri@yahoo.com (A.Y.)

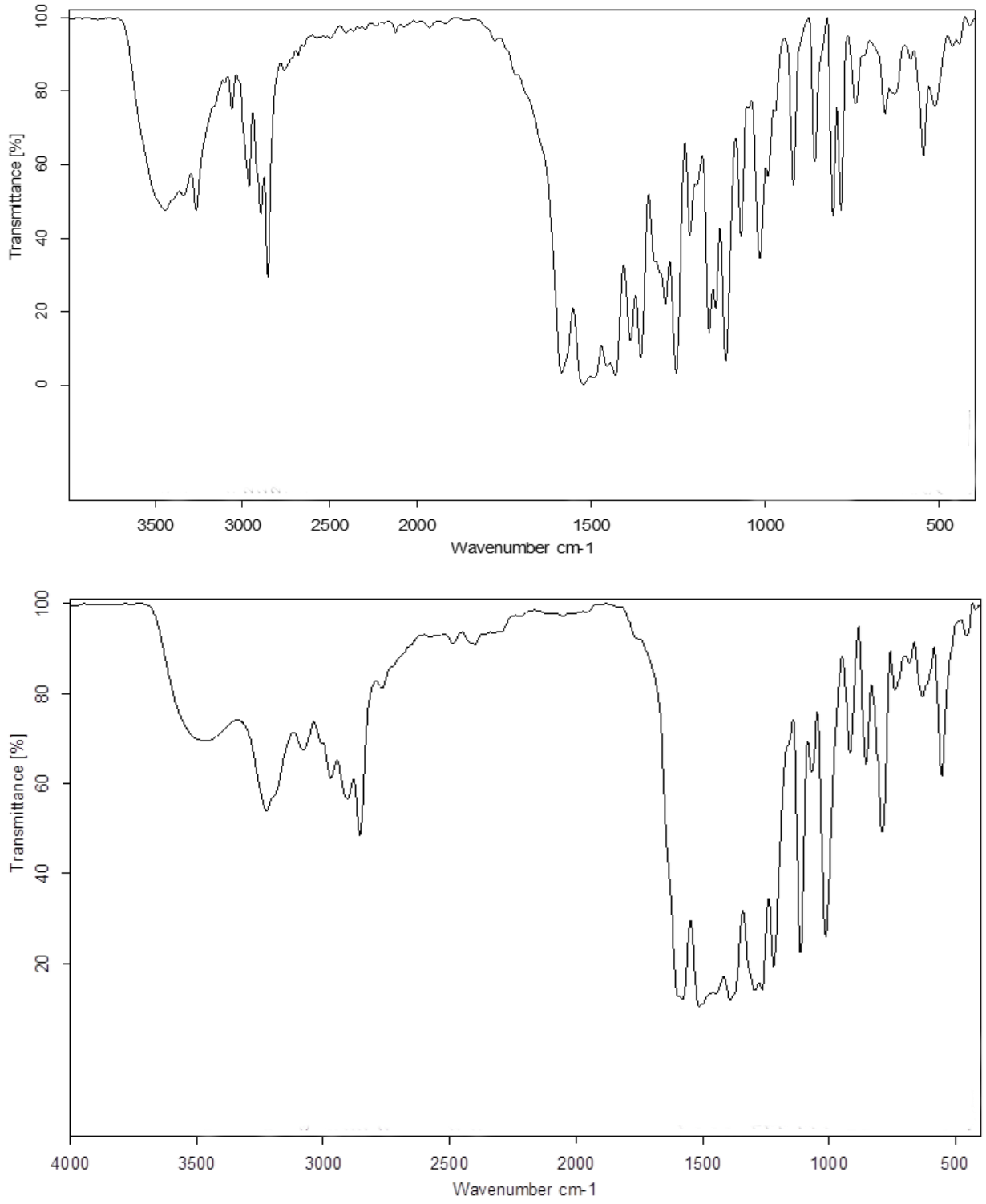


Fig. S1. The FTIR spectra of L (upper) and [ZnL(ONO_2)$_2$]; **1** (lower).

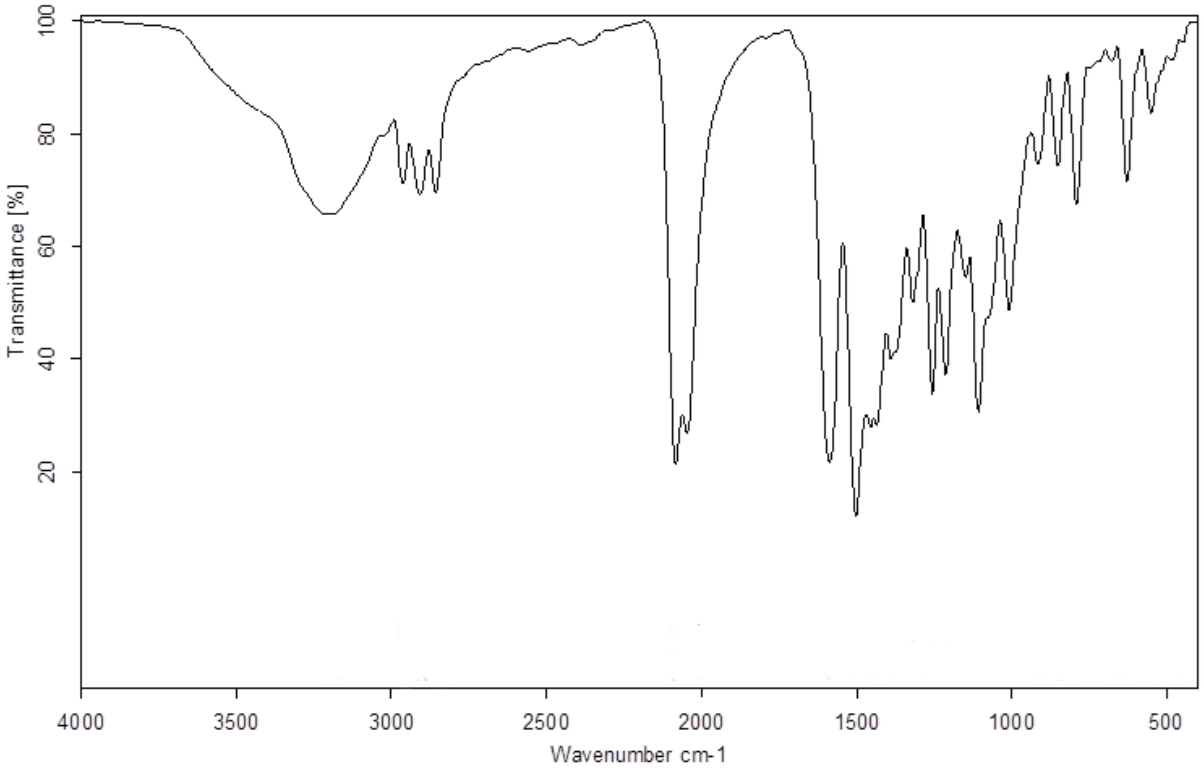


Fig. S2. The FTIR spectra of [ZnL(NCS)$_2$]; **2**.

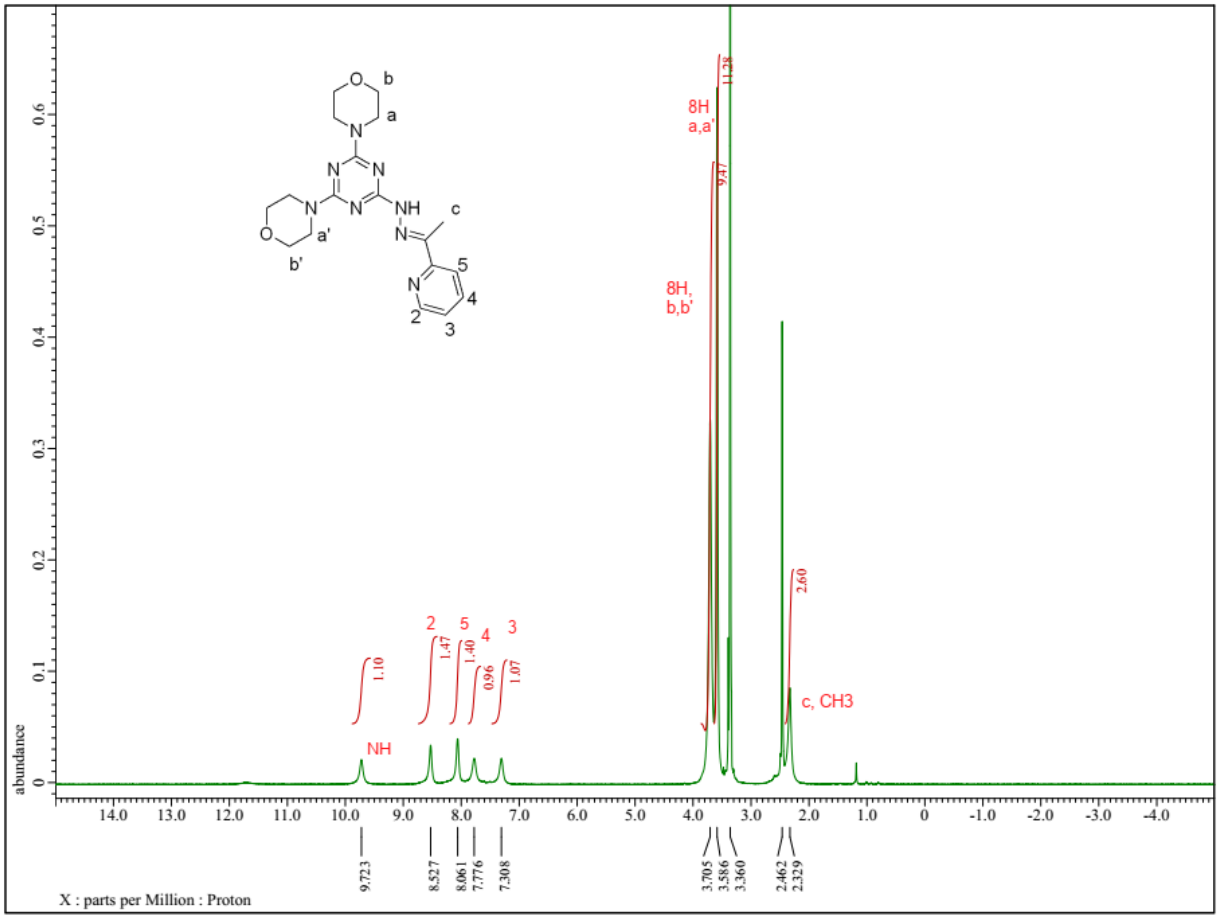


Fig. S3. The ^{1}HNMR spectra of [ZnL(ONO$_2$)$_2$]; **1**.

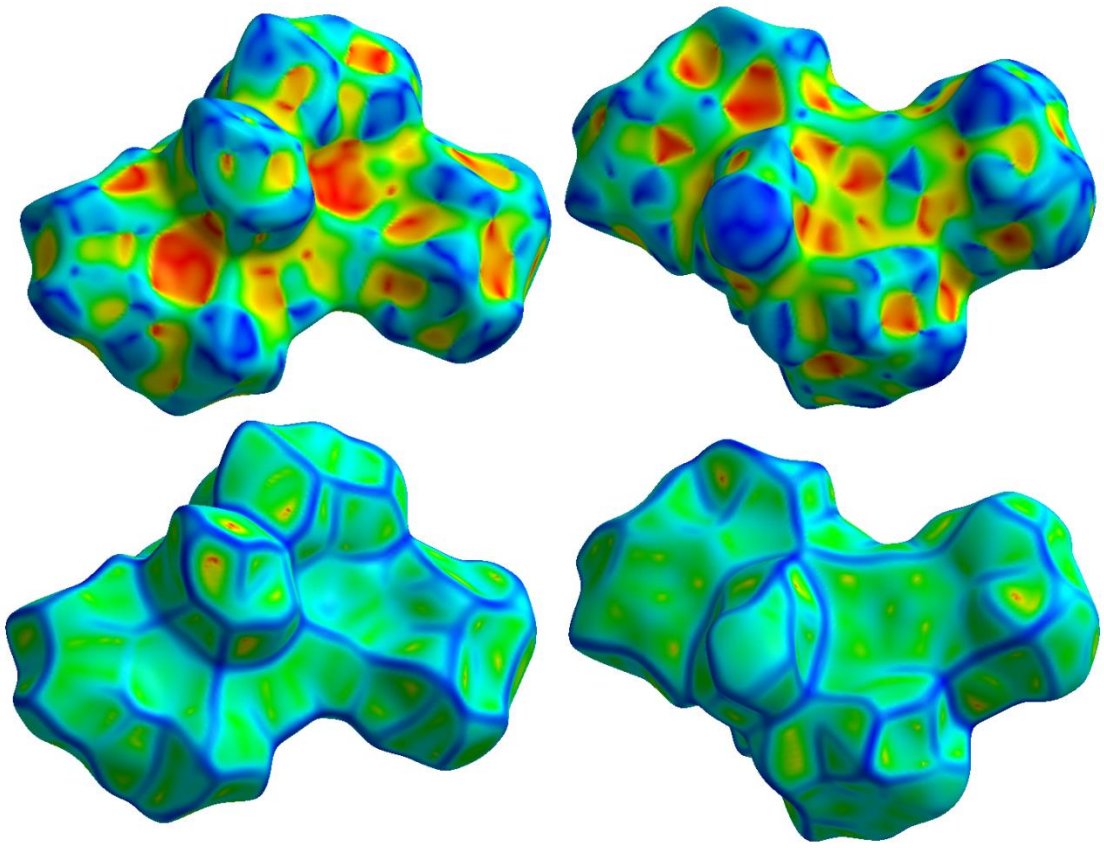


Fig. S4. Shape index and curvedness maps for **1**.

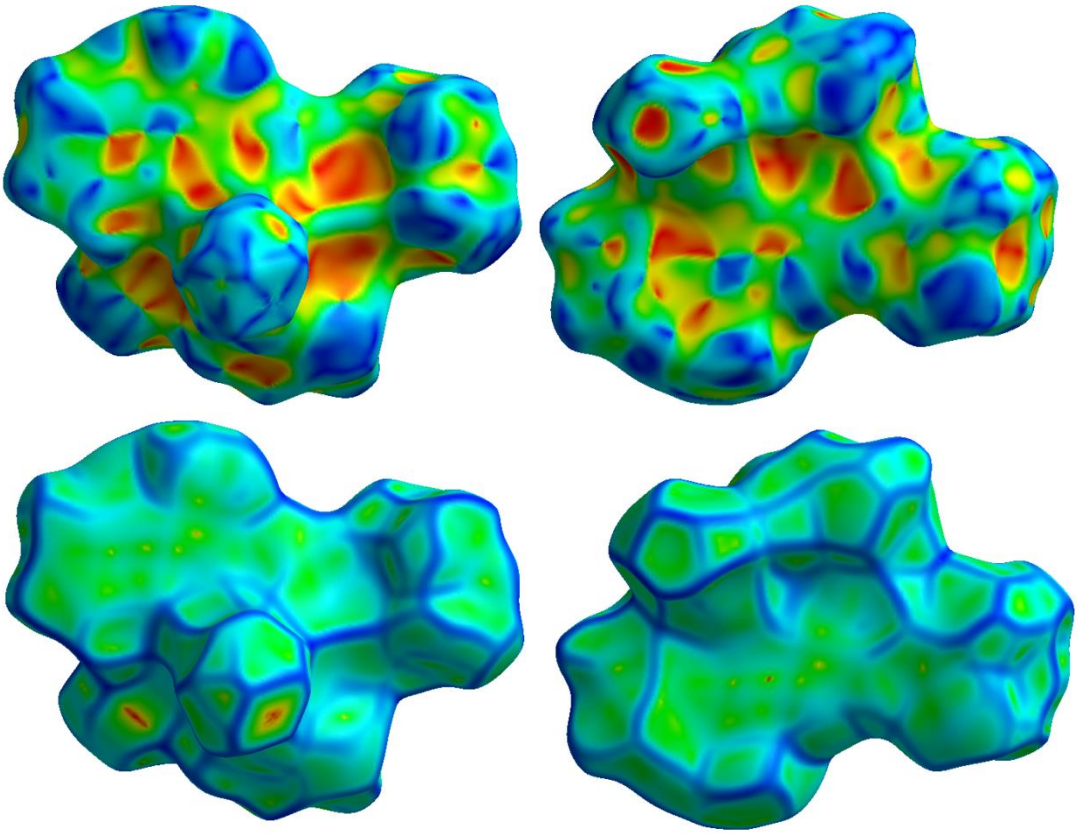


Fig. S5. Shape index and curvedness maps for **2**.

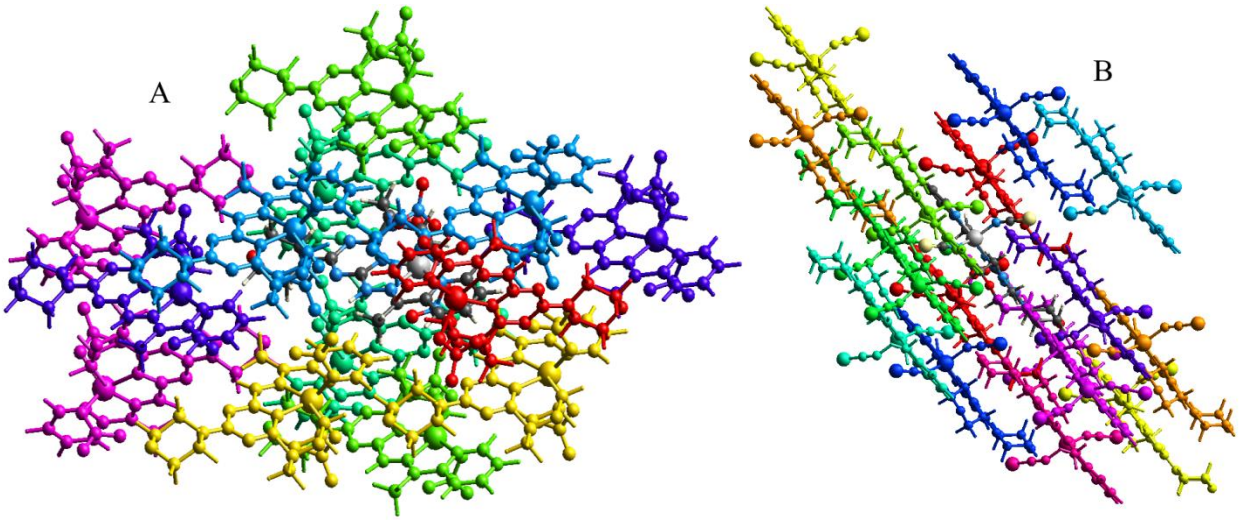


Fig. S6. Visualization of molecular interactions within a cluster with a radius of 3.8 Å between the central molecule under investigation and its neighboring molecules, for **1**; (**A**) and **2**; (**B**).

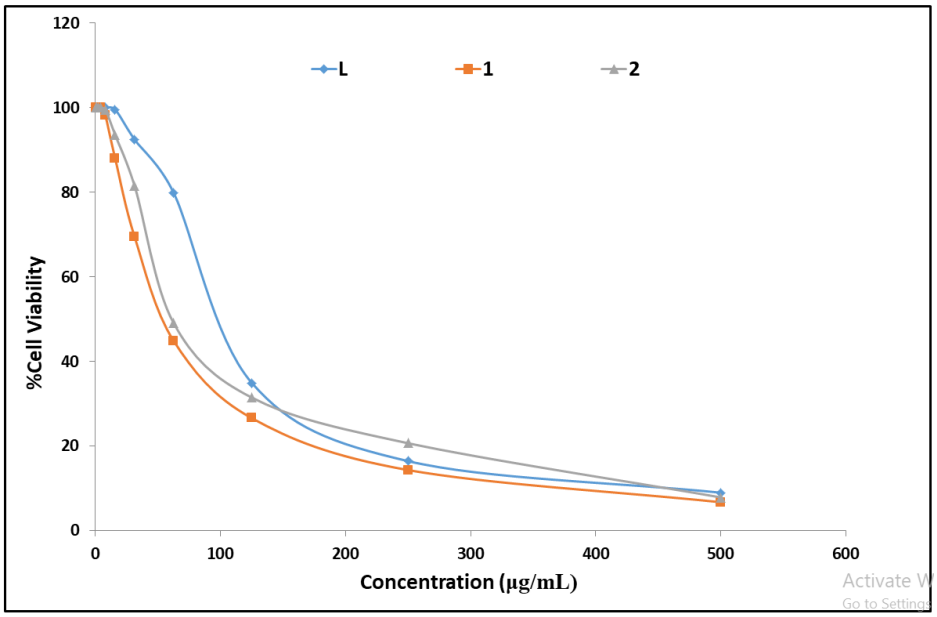


Fig. S7. MTT assay of **1**, **2**, and their **L** ligand against WI-38 normal cells.

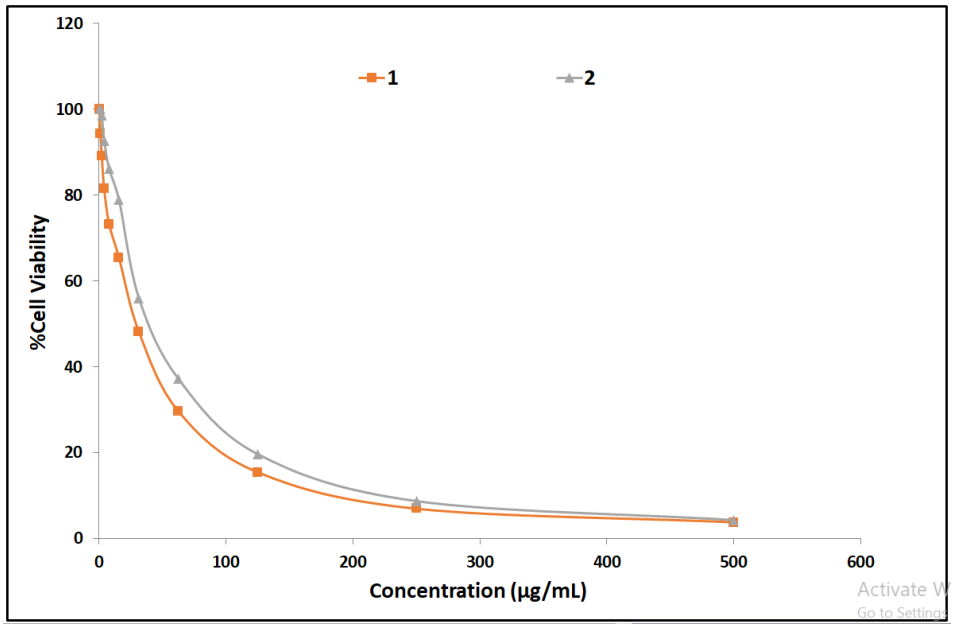


Fig. S8. MTT assay of **1** and **2** against HCT-116 cancerous cells.

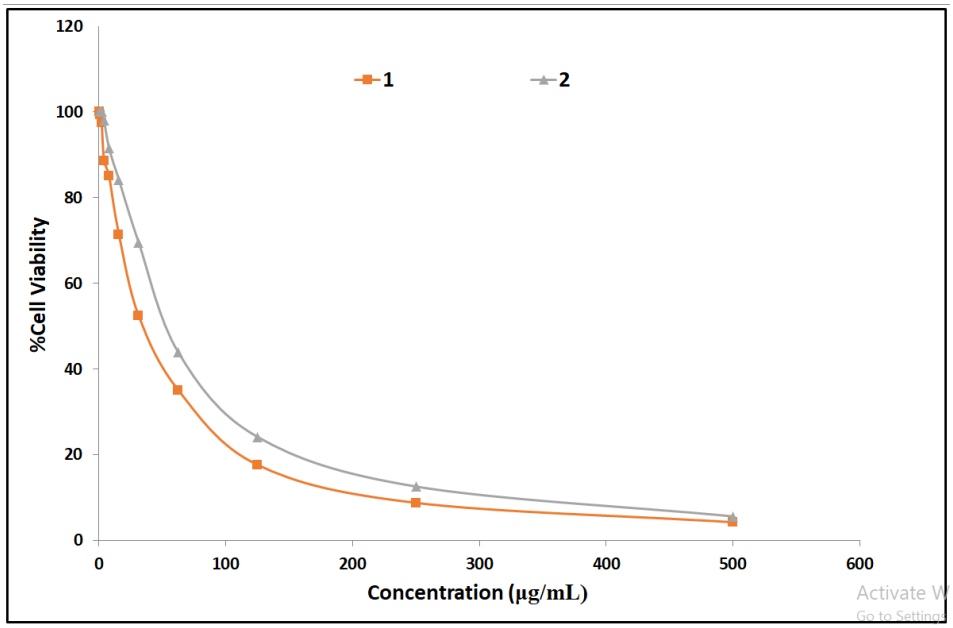


Fig. S9. MTT assay of **1** and **2** against A-549 cancerous cells.

Table S1. Different interaction energies[a] of the molecular pairs in kJ/mol for **1**.

	N	Symop	R	Electron Density	E_{ele}	E_{pol}	E_{dis}	E_{rep}	E_{tot}
	1	-x+1/2, -y, z+1/2	13.18	B3LYP/6-31G(d,p)	-10.1	-2.8	-11.5	0.0	-22.7
	0	-x, y+1/2, -z+1/2	9.57	B3LYP/6-31G(d,p)	-24.2	-14.8	-49.4	31.5	-60.0
	0	x, y, z	7.92	B3LYP/6-31G(d,p)	-10.4	-15.1	-27.6	14.8	-37.1
	2	x+1/2, -y+1/2, -z	9.01	B3LYP/6-31G(d,p)	-20.4	-6.9	-54.9	38.3	-50.9
	0	-x, y+1/2, -z+1/2	7.50	B3LYP/6-31G(d,p)	-70.3	-26.5	-89.5	95.7	-112.8
	0	x, y, z	11.89	B3LYP/6-31G(d,p)	-12.3	-3.9	-20.6	18.8	-22.2
	0	x+1/2, -y+1/2, -z	16.05	B3LYP/6-31G(d,p)	-6.3	-0.4	-5.8	0.0	-12.1

[a]Scale factors of 1.057, 0.740, 0.871 and 0.618 for E_{ele}, E_{pol}, E_{dis} and E_{rep}, respectively.

Table S2. Different interaction energies[a] of the molecular pairs in kJ/mol for **2**.

	N	Symop	R	Electron Density	E_{ele}	E_{pol}	E_{dis}	E_{rep}	E_{tot}
	2	x, -y+1/2, z+1/2	6.34	B3LYP/6-31G(d,p)	-70.0	-32.4	-126.1	103.7	-143.8
	1	x, y, z	13.99	B3LYP/6-31G(d,p)	-0.4	-4.2	-17.6	0.0	-18.8
	1	x, -y+1/2, z+1/2	16.66	B3LYP/6-31G(d,p)	-6.5	-3.1	-11.2	0.0	-18.9
	0	-x, -y, -z	9.64	B3LYP/6-31G(d,p)	-4.5	-13.9	-47.0	40.6	-30.8
	1	-x, y+1/2, -z+1/2	12.35	B3LYP/6-31G(d,p)	-17.4	-4.2	-9.0	0.0	-29.4
	1	-x, -y, -z	10.40	B3LYP/6-31G(d,p)	-6.4	-5.2	-9.9	6.4	-15.2
	0	-x, -y, -z	11.74	B3LYP/6-31G(d,p)	9.9	-2.8	-3.7	21.4	18.4
	1	x, y, z	8.97	B3LYP/6-31G(d,p)	-3.7	-8.2	-17.8	14.8	-16.3
	0	-x, -y, -z	8.68	B3LYP/6-31G(d,p)	-41.1	-12.0	-56.8	39.2	-77.6
	1	-x, y+1/2, -z+1/2	13.28	B3LYP/6-31G(d,p)	-2.6	-2.9	-12.5	0.0	-15.8
	1	-x, -y, -z	13.18	B3LYP/6-31G(d,p)	2.8	-0.9	-8.7	0.0	-5.3

[a]Scale factors of 1.057, 0.740, 0.871 and 0.618 for E_{ele}, E_{pol}, E_{dis}, and E_{rep}, respectively.

Table S3. The NBO analysis for the Zn-N and Zn-O interactions in complexes **1** and **2**.

Donor NBO	Acceptor NBO	E_{int}	Donor NBO	Acceptor NBO	E_{int}
Complex 1			**Complex 2**		
LP(1)N1	LP*(6)Zn1	27.48	LP(1)N3	LP*(6)Zn1	23.79
LP(1)N1	LP*(9)Zn1	34.53	LP(1)N3	LP*(9)Zn1	40.15
LP(1)N2	LP*(6)Zn1	36.39	LP(1)N4	LP*(6)Zn1	27.28
LP(1)N2	LP*(8)Zn1	32.97	LP(1)N4	LP*(8)Zn1	57.34
LP(1)N4	LP*(6)Zn1	41.27	LP(1)N6	LP*(6)Zn1	26.89
LP(1)N4	LP*(9)Zn1	29.10	LP(1)N6	LP*(9)Zn1	38.97
LP(2)O3	LP*(6)Zn1	40.64	LP(1)N1	LP*(6)Zn1	71.84
LP(2)O3	LP*(7)Zn1	27.45	LP(1)N1	LP*(7)Zn1	63.84
LP(2)O3	LP*(8)Zn1	22.54	LP(1)N1	LP*(8)Zn1	9.38
LP(1)O3	LP*(8)Zn1	10.45	LP(1)N2	LP*(6)Zn1	74.15
LP(3)O4	LP*(9)Zn1	5.09	LP(1)N2	LP*(7)Zn1	53.49
LP(2)O4	LP*(6)Zn1	10.27	LP(1)N2	LP*(8)Zn1	12.4
LP(1)O4	LP*(7)Zn1	9.19			
LP(2)O4	LP*(7)Zn1	14.05			
LP(2)O6	LP*(6)Zn1	40.42			
LP(2)O6	LP*(7)Zn1	33.1			
LP(2)O6	LP*(8)Zn1	21.87			
LP(1)O6	LP*(8)Zn1	11.38			
LP(3)O6	LP*(9)Zn1	5.24			
LP(1)O7	LP*(7)Zn1	8.3			
LP(2)O7	LP*(7)Zn1	8.19			

Table S4. Evaluation of cytotoxicity against WI-38 cell line for **L**.

Sample conc. (µg/mL)	Viability %	Inhibitory %	S.D. (±)[a]
500	8.97	91.03	0.81
250	16.43	83.57	1.29
125	34.91	65.09	1.35
62.5	79.85	20.15	1.41
31.25	92.46	7.54	0.62
15.6	99.58	0.42	0.23
7.8	100	0	
3.9	100	0	
2	100	0	
1	100	0	
0	100	0	

[a] Standard deviation IC_{50} = 104.01±3.61 µg/mL

Table S5. Evaluation of cytotoxicity against WI-38 cell line for **1**.

Sample conc. (µg/mL)	Viability %	Inhibitory %	S.D. (±)[a]
500	6.71	93.29	0.35
250	14.32	85.68	1.06
125	26.59	73.41	0.97
62.5	44.85	55.15	1.31
31.25	69.43	30.57	1.65
15.6	88.06	11.94	0.62
7.8	98.12	1.88	0.34
3.9	100	0	
2	100	0	
1	100	0	
0	100	0	

[a] Standard deviation IC_{50} = 55.95±1.86 µg/mL

Table S6. Evaluation of cytotoxicity against WI-38 cell line for **2**.

Sample conc. (µg/mL)	Viability %	Inhibitory %	S.D. (±)[a]
500	7.85	92.15	0.61
250	20.67	79.33	0.35
125	31.45	68.55	0.64
62.5	49.03	50.97	1.29
31.25	81.48	18.52	0.86
15.6	93.62	6.38	0.34
7.8	99.57	0.43	0.19
3.9	100	0	
2	100	0	
1	100	0	
0	100	0	

[a] Standard deviation IC_{50} = 61.57±2.17 µg/mL

Table S7. Evaluation of cytotoxicity activity against HCT-116 cell line for **1**.

Sample conc. (µg/mL)	Viability %	Inhibitory %	S.D. (±)[a]
500	3.79	96.21	0.16
250	6.95	93.05	0.23
125	15.43	84.57	0.79
62.5	29.61	70.39	1.43
31.25	48.16	51.84	2.08
15.6	65.39	34.61	1.75
7.8	73.22	26.78	0.84
3.9	81.45	18.55	0.97
2	89.21	10.79	0.45
1	94.36	5.64	0.42
0	100	0	

[a] Standard deviation IC_{50} = 29.53±1.24 µg/mL

Table S8. Evaluation of cytotoxicity activity against HCT-116 cell line for **2**.

Sample conc. (µg/mL)	Viability %	Inhibitory %	S.D. (±)[a]
500	3.79	96.21	0.16
250	6.95	93.05	0.23
125	15.43	84.57	0.79
62.5	29.61	70.39	1.43
31.25	48.16	51.84	2.08
15.6	65.39	34.61	1.75
7.8	73.22	26.78	0.84
3.9	81.45	18.55	0.97
2	89.21	10.79	0.45
1	94.36	5.64	0.42
0	100	0	

[a] Standard deviation IC_{50} = 29.53±1.24 µg/mL

Table S9. Evaluation of cytotoxicity activity against A-549 cell line for **1**.

Sample conc. (µg/mL)	Viability %	Inhibitory %	S.D. (±)[a]
500	4.27	95.73	0.19
250	8.78	91.22	0.44
125	17.64	82.36	0.72
62.5	35.07	64.93	0.91
31.25	52.38	47.62	1.26
15.6	71.42	28.58	0.34
7.8	85.09	14.91	0.65
3.9	88.65	11.35	0.31
2	97.42	2.58	0.16
1	99.23	0.77	0.15
0	100	0	

[a] Standard deviation IC_{50} = 35.55±1.69 µg/mL

Table S10. Evaluation of cytotoxicity activity against A-549 cell line for **2**.

Sample conc. (µg/mL)	Viability %	Inhibitory %	S.D. (±)[a]
500	5.63	94.37	0.15
250	12.59	87.41	0.73
125	24.16	75.84	0.92
62.5	43.89	56.11	1.45
31.25	69.51	30.49	1.33
15.6	84.17	15.83	1.09
7.8	91.59	8.41	0.37
3.9	98.03	1.97	0.21
2	100	0	
1	100	0	
0	100	0	

[a] Standard deviation IC_{50} = 55.05±2.87 µg/mL

Experimental details:

Materials and physical characterizations

All chemicals and solvents were procured from Sigma-Aldrich Chemical Company Inc. (St. Louis, MO, USA) and used without further purification. FTIR spectra were acquired using a Bruker Tensor 37 FTIR instrument (Bruker, Germany) with the KBr disc method, recording spectra in the range 4000–400 cm^{-1}. CHN analysis was performed using a PerkinElmer 2400 Elemental Analyzer (PerkinElmer Inc., Waltham, MA, USA). Zn content was determined using a Shimadzu atomic absorption spectrophotometer (AA7000 series, Shimadzu, Ltd., Kyoto, Japan).

X-Ray structure determinations

The crystals of **1** and **2** were immersed in cryo-oil, mounted in a loop, and measured at a temperature of 120 K. The X-ray diffraction data were collected on a Rigaku Oxford Diffraction Supernova diffractometer using Cu Kα radiation. The *CrysAlisPro* [36] software package was used for cell refinements and data reductions. A gaussian absorption correction (*CrysAlisPro* [36]) was applied to the intensities before the structure solutions. The structures were solved by the intrinsic phasing (*SHELXT* [37]) method. Structural refinements were carried out using *SHELXL* [38] software with *Olex2* [39] graphical user interface. Structure **1** was solved in chiral space group $P2_12_12_1$. In **1** the hydrogen atom H3 and in **2** hydrogen atoms H9A, H9B, H9C, H3, H4, H5, and H5A were located from the difference Fourier map and refined isotropically. All other hydrogen atoms were positioned geometrically and constrained to ride on their parent atoms, with C-H = 0.95-0.99 Å and U_{iso} = 1.2-1.5·U_{eq}(parent atom).

Method S1. Evaluation of cytotoxicity activity [63**]**

Cell line Propagation

The cells were obtained from the American Type Culture Collection (ATCC, Rockville, MD) and propagated in Dulbecco's modified Eagle's medium (DMEM) supplemented with 10% heat-inactivated fetal bovine serum, 1% L-glutamine, HEPES buffer and 50 μg/mL Gentamycin. Cells were maintained at 37ºC in a humidified atmosphere with 5% CO_2 and were subcultured two times a week.

Cytotoxicity evaluation using viability assay

For cytotoxicity assay, the cells were seeded in 96-well plate at a cell concentration of 1×10^4 cells per well in 100 μl of growth medium. Fresh medium containing different concentrations of the test sample was added after 24 h of seeding. Serial two-fold dilutions of the tested chemical compound were added to confluent cell monolayers dispensed into 96-well, flat-bottomed microtiter plates (Falcon, NJ, USA) using a multichannel pipette. The microtiter plates were incubated at 37ºC in a humidified incubator with 5% CO_2 for a period of 24 h. Three wells were used for each concentration of the test sample. Control cells were incubated without test sample and with or without DMSO. The little percentage of DMSO present in the wells (maximal 0.1%) was found not to affect the experiment. After incubation of the cells for at 37°C, for 24 h, the viable cells yield was determined by the MTT test. Briefly, the media was removed from the 96 well plate and replaced with 100 μL of fresh culture DMEM medium without phenol red then 10 μL of the 12 mM MTT stock solution (5 mg of MTT in 1 mL of PBS) to each well including the untreated controls. The 96-well plates were then incubated at 37°C and 5% CO_2 for 4 h. An 85 μL aliquot of the media was removed from the wells, and 50 μL of DMSO was added to each well and mixed thoroughly with the pipette and incubated at 37°C for 10 min. Then, the optical density was measured at 590 nm with the microplate reader (SunRise, TECAN, Inc, USA) to determine the number of viable cells and the percentage of viability was calculated as [(ODt/ODc)]x100% where ODt is the mean optical density of wells treated with the tested sample and ODc is the mean optical density of untreated cells. The relation between surviving cells and drug concentration is plotted to get the survival curve of each tumor cell line after treatment with the specified compound. The 50% inhibitory concentration (IC_{50}), the concentration required to cause toxic effects in 50% of intact cells, was estimated from graphic

plots of the dose response curve for each concentration using Graphpad Prism software (San Diego, CA. USA).

Method S2. Evaluation of antimicrobial activity [64**]**

a) Tested pathogenic microbes

The antimicrobial activity was evaluated against two gram-positive bacteria ((*S. aureus* (ATCC 25923) and *B. subtilis* (RCMB015(1)NRR LB-543)), two gram-negatvie bacteria ((*E. coli* (ATCC 25922) and *P. vulgaris* (RCMB 004(1)ATCC 13315)) and two fungi ((*A. fumigatus* (RCMB 002008) and *C. albicans* (RCMB 005003(1) ATCC 10231)). Gentamycin was used as standard antibacterial agent. The samples maintained in Brain heart infusion (BHI) at 20ºC; 300 mL of each stock-culture was added to 3 mL of BHI broth. Overnight cultures were kept for 24 h at 37 ºC±1ºC and the purity of cultures was checked after 24 h of incubation. After 24 h of incubation, bacterial suspension was diluted with sterile physiological solution, for the diffusion and indirect bioautographic tests, to 108 CFU/mL (turbidity = McFarland barium sulfate standard 0.5). In case of fungi *A. fumigatus* (RCMB 002008) and *C. albicans* (RCMB 005003(1) ATCC 10231), the used medium in antagonistic activity against tested fungi is Potato Dextrose Agar, where Ketoconazole was used standard antifungal agent.

b) Agar well diffusion method

Synthetic compound was prepared at concentration 10 mg/mL dissolved in DMSO as stock solutions. Preparation of sterilized Mueller Hinton agar plates seeded with tested pathogenic bacteria occurred. The wells are done by sterilized cork borer in size 6 mm and hence 100 µL of the synthetic compound was poured in each well comparably with DMSO as control. The plates were incubated at 37°C for 24-48 h (for bacteria) and at 28°C for 48 h (for fungi). After incubation period; antimicrobial activity was determined by inhibition zones.

C) Minimum Inhibitory Concentration (MIC)

Different dilutions of the compound are inoculated with tested pathogenic microbes. After incubation period of 96-well microplate, the results are measured using microplate reader. To determine at what level the MIC endpoint is established; subculture of test samples at different concentrations occurred in nutrient agar plates.

Method S3. Energy framework analysis protocol [40-51]

The energy framework is crucial for understanding the various energy types involved in the supramolecular assembly of molecules within a crystal. This technique involves calculating and comparing various energy components such as repulsion (E_{rep}), electrostatic (E_{ele}), dispersion (E_{dis}), polarization (E_{pol}), and total (E_{tot}) energy. These calculations are based on the anisotropy of the topology of pairwise intermolecular interaction energies. They encompass electrostatic energy, which deals with the forces between charged particles; polarization energy, which arises from the distortion of a molecule's electron cloud by nearby charge distributions; dispersive energy, which involves weak attractive forces resulting from temporary fluctuations in a molecule's electron distribution; and repulsive energy, which is the energy needed to overcome the forces preventing two molecules from interacting. The total interaction energy of the molecule is the sum of these different interaction energies, as represented in the following formula:

$$E_{tot} = E_{ele} + E_{pol} + E_{dis} + E_{rep}$$

In the analysis of the title compounds, the Crystal Explorer program was utilized to determine the energy framework. The computational approach involved generating new wave functions. The energy framework is represented by cylinders, with the thickness of the cylinders indicating the strength of interactions. The thickness is directly proportional to the energy magnitude, providing valuable insights into the stabilization of the crystal packing. The calculations were based on the B3LYP/6-31G(d,p) accurate level of theory, and the software facilitated the calculation of interaction energies for a 3.8 Å cluster around a single molecule, using scale factors consistent with established values. The resulting three-dimensional energy frameworks were visualized to emphasize neighboring molecules within a 3.8 Å radius from the reference molecule (**Fig. S5**). The data presented in **Table S1** and **S2** for the energy frameworks illustrate the contributions of different components, including E_{ele}, E_{pol}, E_{dis}, E_{rep}, and E_{tot}, to various intermolecular interactions in each compound. Additionally, the calculations involved symmetry operations to construct molecular wavefunctions and estimate electron densities, enabling the calculation of electrostatic, polarization, dispersion, and exchange-repulsion energy components.

This approach provided valuable insights into the organization of the tested compounds within their crystal structures. Also, **Table S1** and **S2** not only provides an energy breakdown but also details such as the color-coding scheme corresponding to molecular interactions at specific Cartesian coordinates. It includes components of the interaction energies (E), the number of pairs of interacting molecules with the reference molecule (N), the centroid-to-centroid distance between the reference molecule and interacting molecules (R), and the associated rotational symmetry operations (symmetry). These details are crucial for lattice energy calculations.

References

40. Turner, M.J.; Thomas, S.P.; Shi, M.W.; Jayatilaka, D.; Spackman, M.A. Energy frameworks: insights into interaction anisotropy and the mechanical properties of molecular crystals. *Chem. Commun.* **2015**, *51*, 3735-3738.

41. Bakheit, A.H.; Attwa, M.W.; Kadi, A.A.; Alkahtani, H.M. Structural Analysis and Reactivity Insights of (*E*)-Bromo-4-((4-((1-(4-chlorophenyl)ethylidene)amino)-5-phenyl-4H-1,2,4-triazol-3-yl)thio)-5-((2-isopropylcyclohexyl)oxy) Furan-2(5H)-one: A combined approach using single-crystal X-ray diffraction, Hirshfeld surface analysis, and conceptual density functional theory. *Crystals* **2023**, *13*, 1313.

42. Turner, M.J.; Grabowsky, S.; Jayatilaka, D.; Spackman, M.A. Accurate and efficient model energies for exploring intermolecular interactions in molecular crystals. *J. Phys. Chem. Lett.* **2014**, *5*, 4249-4255.

43. Hajji, M.; Mtiraoui, H.; Amiri, N.; Msaddek, M.; Guerfel, T. Crystallographic and first-principles density functional theory study on the structure, noncovalent interactions, and chemical reactivity of 1,5-benzodiazepin-2-ones derivatives. *Int. J. Quantum Chem.* **2019**, *119*, e26000.

44. Abad, N.; Sallam, H.H.; Al-Ostoot, F.H.; Khamees, H.A.; Al-horaibi, S.A.; Khanum, S.A.; Madegowda, M.; El Hafi, M.; Mague, J.T.; Essassi, E.M. Synthesis, crystal structure, DFT calculations, Hirshfeld surface analysis, energy frameworks, molecular dynamics and docking studies of novel isoxazolequinoxaline derivative (IZQ) as anti-cancer drug. *J. Mol. Struct.* **2021**, *1232*, 130004.

45. Edwards, A.J.; Mackenzie, C.F.; Spackman, P.R.; Jayatilaka, D.; Spackman, M.A. Intermolecular interactions in molecular crystals: what's in a name? *Faraday Discuss.* **2017**, *203*, 93-112.

46. Mackenzie, C.F.; Spackman, P.R.; Jayatilaka, D.; Spackman, M.A. CrystalExplorer model energies and energy frameworks: extension to metal coordination compounds, organic salts, solvates and open-shell systems. *IUCrJ* **2017**, *4*, 575-587.

47. Wang, K.; He, X.; Rong, C.; Zhong, A.; Liu, S.; Zhao, D. On the origin and nature of internal methyl rotation barriers: An information-theoretic approach study. *Theor. Chem. Acc.* **2022**, *141*, 68.

48. Zhong, A.; Chen, D.; Li, R. Revisiting the beryllium bonding interactions from energetic and wavefunction perspectives. *Chem. Phys. Lett.* **2015**, *633*, 265-272.

49. Tan, S.L.; Jotani, M.M.; Tiekink, E.R. Utilizing Hirshfeld surface calculations, non-covalent interaction (NCI) plots and the calculation of interaction energies in the analysis of molecular packing. *Acta Crystallogr. E: Crystallogr. Commun.* **2019**, *75*, 308-318.

50. Sreenatha, N.; Chakravarthy, A.J.; Suchithra, B.; Lakshminarayana, B.; Hariprasad, S.; Ganesha, D. Crystal, spectral characterization, molecular docking, Hirshfeld computational studies and 3D-energy framework analysis of a novel puckered compound ($C_{14}H_{15}ClO$): 2-Chloro-3-phenyl-5,5-dimethylcyclohex-2-en-1-one. *J. Mol. Struct.* **2020**, *1210*, 127979.

51. Guo, Z.A.; Xian, J.Y.; Rong, L.R.; Qin, H.; Jie, Z. Theoretical study of metal ion impact on geometric and electronic properties of terbutaline compounds. *Monatsh. Chem.* **2019**, *150*, 1355-1364.

54. Rikagu Oxford Diffraction. CrysAlisPro 1.171.43.100a, **2023**; Rikagu Oxford Diffraction Inc.: Yarnton, Oxfordshire, England.

55. Sheldrick, G. M. *Acta Cryst.* **2015**, *A71*, 3-8.

56. Sheldrick, G. M. *Acta Cryst.* **2015**, *C71*, 3-8.

57. Dolomanov, O. V., Bourhis, L. J., Gildea, R. J, Howard, J. A. K., Puschmann, H. *J. Appl. Cryst.* **2009**, *42*, 339-341.

63. Mosmann, T. Rapid colorimetric assay for cellular growth and survival: application to proliferation and cytotoxicity assays. *J. Immunol. Methods* **1983**, *65*, 55-63.

64. Lu, P.-L.; Liu, Y.-C.; Toh, H.-S.; Lee, Y.-L.; Liu, Y.-M.; Ho, C.-M.; Huang, C.-C.; Liu, C.-E.; Ko, W.-C.; Wang, J.-H. Epidemiology and antimicrobial susceptibility profiles of gram-negative bacteria causing urinary tract infections in the Asia-Pacific region: 2009–2010 results from the Study for Monitoring Antimicrobial Resistance Trends (SMART). *Int. J. Antimicrob. Agents* **2012**, *40*, S37-S43.